PHYSICAL REVIEW D **89,** 074503 (2014)

Gluon screening mass at finite temperature from the Landau gauge gluon propagator in lattice QCD

P. J. Silva,[*] and O. Oliveira[†]

CFC, Departamento de Física, Faculdade de Ciências e Tecnologia, Universidade de Coimbra, 3004-516 Coimbra, Portugal

P. Bicudo,[‡] and N. Cardoso[§]

CFTP, Departamento de Física, Instituto Superior Técnico, Avenida Rovisco Pais, 1049-001 Lisboa, Portugal

(Received 22 October 2013; published 2 April 2014)

We address the interpretation of the Landau gauge gluon propagator at finite temperature as a massive-type bosonic propagator. Using pure gauge SU(3) lattice simulations at a fixed lattice volume $\sim(6.5\ \mathrm{fm})^3$, we compute the electric and magnetic form factors, extract a gluon mass from Yukawa-like fits, and study its temperature dependence. This is relevant both for the Debye screening at high temperature T and for confinement at low T.

DOI: 10.1103/PhysRevD.89.074503 PACS numbers: 11.15.Ha, 11.10.Wx, 14.70.Dj

I. INTRODUCTION

Finite temperature $SU(3)$ pure Yang-Mills theory has a first-order transition at the critical temperature $T = T_c \sim 270$ MeV [1,2]. For temperatures below T_c gluons are confined, i.e., do not behave as free particles. On the other hand, for $T > T_c$ gluons become deconfined and, for sufficiently high T, they can be treated perturbatively [3,4]. The order parameter for the confinement-deconfinement phase transition is the Polyakov loop P_L, a path ordered product of exponentials of the gluon field time-like component. For $T < T_c$ the center symmetry of gauge group is unbroken and $P_L = 0$. On the other hand, for $T > T_c$ the center symmetry is spontaneously broken and $P_L \neq 0$. This change in the behavior of the Polyakov loop with temperature is rooted in the gluodynamics and should also be seen in the correlation functions of the gluon fields, such as the gluon propagator.

At zero temperature, the momentum space gluon propagator in the Landau gauge is described by a single scalar function $D(p^2)$. For $T \neq 0$ the propagator requires two scalar functions $D_T(p^2;T)$ and $D_L(p^2;T)$ that are associated with the gluon transverse and longitudinal degrees of freedom, respectively. Recently, a number of lattice QCD simulations dedicated to the study of the two point gluon correlation function (see, for example, [5–18] and references therein) have shown that $D_L(p^2;T)$ and $D_T(p^2;T)$ are nontrivial functions of T and that their nature changes as T crosses T_c. Indeed, in [10,12] the authors identify possible order parameters for the confinement-deconfinement phase transition directly related with the gluon propagator.

The lattice QCD simulations show that the electric $D_L(p^2;T)$ and magnetic $D_T(p^2;T)$ form factors are finite for all momenta and temperatures. An interpretation of the gluon propagator form factors in terms of quasiparticle massive bosons is welcome when building effective models to describe the hadronic phase diagram [19,20] and also provides a check to the temperature dependent perturbative approach to QCD [21–23].

A gluon screening mass can be identified with the pole of the gluon two point correlation function in momentum space or, in real space, with the exponential decay of the propagator at large distances. Although the gluon propagator is not gauge invariant, it has been conjectured that the gluon screening mass associated with the longitudinal degrees of freedom, i.e., the Debye gluon mass, is independent of the gauge [24–36]. At finite temperature, the Debye mass is related to the screening of the color interaction which is expected to occur at high T [21–23]. Note that at zero temperature, a finite and nonvanishing gluon mass is linked with gluon confinement [37–39].

Above the deconfinement temperature of QCD, finite temperature field theory, see, e.g., [3,4,40], treats the gluons as an ideal gas of massive particles. The electric propagator acquires a pole which defines the gluon Debye mass $m_D \sim gT$, where g is the strong coupling constant. For example, m_D is used in Boltzmann models for heavy ion interactions [41]. Similarly, for the transverse degrees of freedom, one can define a magnetic mass $\sim g^2 T$ (see, e.g., [40]).

The Debye mass can be computed in $SU(N)$ using perturbation theory and, to next-to-leading order in the strong coupling constant g, is given by [42]

[*]psilva@teor.fis.uc.pt
[†]orlando@fis.uc.pt
[‡]bicudo@ist.utl.pt
[§]Present address: NCSA, University of Illinois, Urbana IL 61801, USA.
nunocardoso@cftp.ist.utl.pt

$$\frac{m_D}{gT} = \frac{N}{3} + g\left[\alpha + \frac{N}{4\pi}\log\left(\frac{N}{3g}\right)\right] + \mathcal{O}(g^2), \qquad (1)$$

where α is a nonperturbative constant, in the sense that it is not computable within perturbation theory. For very high temperatures and up to $T \sim 10^4 T_c$, m_D was measured using lattice simulations for the gauge group SU(2) [43]. The simulations show $m_D \propto T$ and an α, associated with the slope of $m_D(T)$, that is large for all T's. Moreover, the static quark-antiquark free energy has been computed at finite T using lattice QCD and the mass dimension screening parameter of the quark-antiquark potential is compatible with a linear T behavior [44–53].

For large T, the color interaction is suppressed due to a Debye mass $m_D \neq 0$. However, near the critical temperature T_c it is not clear what value it should take [54]. Pure gauge QCD has a first order phase transition at $T_c = 270$ MeV and this suggests a vanishing gluon mass at $T = T_c$. However, recently [20], using the experimental data for heavy ions and, in particular, the kaon to pion multiplicity ratio, a finite gluon mass $m_g = 0.32 \pm 0.07$ GeV was estimated at T_c.

On the other hand, the analogy between QCD and superconductors leads to a dual massive gluon at low temperature $T \sim 0$. In superconductors, the screening of the magnetic field in the London equation has a direct relation with an effective mass, the inverse of the magnetic penetration length, of the interaction particle, i.e., the photon. The dual gluon mass was studied using lattice QCD techniques in [55–61]; see, e.g., [62] for a review on the dual gluon and gluon effective masses computed using several nonperturbative approaches. Recently, the penetration length started to be computed with gauge invariant lattice QCD techniques [62–64]. If some constituent gluon models assume a vanishing gluon mass [65–74] at $T \sim 0$, others consider a constituent gluon with a finite mass [75–80]. For an infrared gluon mass in the range 0.5 to 1.0 GeV, the constituent massive gluon models are also consistent with the large glueball masses as predicted by lattice QCD [81–109].

A nonvanishing gluon mass is clearly a nonperturbative feature of QCD. For example, at zero temperature and in perturbation theory, the gluon mass m_g, taken as a pole in the propagator, vanishes to all orders. At zero temperature, the decoupling solution of the Dyson-Schwinger equations [37,110] generates a running effective gluon mass $m_g(p^2)$. Furthermore, lattice QCD results [39] are compatible with the same type of running mass.

In this paper, we compute gluon masses $m_g(T)$, associated with the longitudinal and transverse gluon propagator form factors, for various temperatures and up to $2T_c$ using lattice QCD simulations. The gluon mass is identified by modeling the lattice data [12,43,111], and we consider two different definitions: (i) an infrared pole mass assuming a Yukawa functional form and (ii) a generalization of the functional form which reproduces the zero temperature lattice and Dyson-Schwinger propagators [37,39,110]. Furthermore, we also investigate the mass scale associated with the zero momentum form factors. As discussed in [12], we confirm that this mass scale can also be used as an order parameter for the confinement-deconfinement phase transition.

Ideally, one would like to access the full complex p^2 plane to determine the poles of the propagator. This is a nontrivial problem that would require, for example, the computation of the spectral density as discussed in [112–114]. The analytic structure of the gluon propagator has also been investigated within the Dyson-Schwinger approach in [115–124]. However, given the approximations involved in the calculation and the difficulty of numerical computation, the outcome of the Dyson-Schwinger equations requires an independent confirmation.

The paper is organized as follows. In Sec. II we detail the lattice QCD setup, the gauge fixing procedure, the computation of the gluon propagator at finite T, the renormalization of the lattice data and comment on the systematics. In Sec. III we summarize our results for the longitudinal and transverse components of the gluon propagator. In Sec. IV we detail our results for the gluon mass as a function of the temperature, taking the various definitions referred in the previous paragraph. Finally in Sec. V we resume and conclude.

II. LATTICE SETUP, GAUGE FIXING, AND THE GLUON PROPAGATOR

The lattice simulations reported here have been performed on a lattice $L_s^3 \times L_t$ using the Wilson gauge action for the gauge group SU(3) and for various β. The temperature is taken as the inverse of the lattice time extension $T = 1/L_t$ in physical units. Note that in this work we consider a constant physical volume $\sim(6.5\ \text{fm})^3$. Given that the typical scale for color interaction is $\sim$1 fm, the finite volume effects are expected to be small.

For converting the simulation results into physical units we rely on [125], where the lattice spacing was set from the string tension for a number of β values. In order to be able to keep the spatial volume at $\sim(6.5\ \text{fm})^3$ and access various T, the results of [125] were fitted to the functional form considered in [126], i.e., to

$$\frac{1}{a(\beta)} = \exp\{b_0 + b_1(\beta - 6) + b_2(\beta - 6)^2 + b_3(\beta - 6)^3\}. \qquad (2)$$

The fit, see Fig. 1, gives $b_0 = 0.6702(87)$, $b_1 = 1.768(21)$, $b_2 = -0.68(10)$ and $b_3 = 0.29(14)$ for a $\chi^2/\text{d.o.f.} = 0.027$. In the following, we will always use the relation $a(\beta)$ as given by Eq. (2).

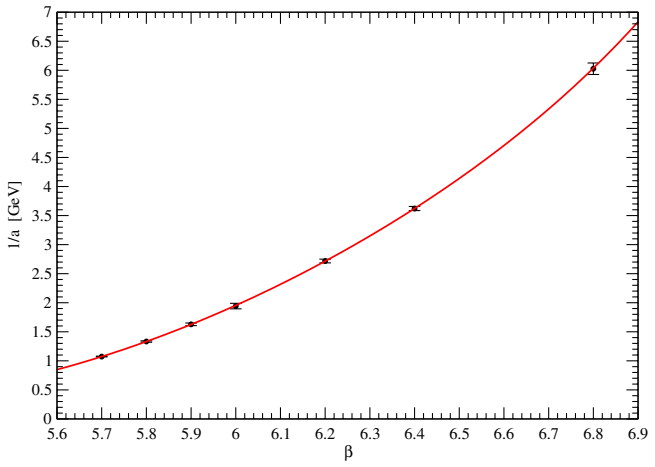

FIG. 1 (color online). $1/a(\beta)$ data from [125] and the fit to Eq. (2).

The lattice setup considered in the current work is described in Table I. The generation of the gauge configurations was done using the Chroma library [127].

A. Landau gauge fixing

In lattice QCD, the fundamental fields are the link variables $U_\mu(x) \in \mathrm{SU}(3)$, which are related to the gluon fields A_μ^a by

$$U_\mu(x) = \exp\{iag_0 A_\mu(x + a\hat{e}_\mu/2)\}; \tag{3}$$

$\hat{e}_\mu$ are unit vectors along the μ direction. In QCD the fields related by gauge transformations,

TABLE I. Lattice setup used for the computation of the gluon propagator at finite temperature. The β was adjusted to have $L_s a \simeq 6.5$ fm. See text for details.

Temp. (MeV)	β	L_s	L_t	a (fm)	$1/a$ (GeV)
121	6.0000	64	16	0.1016	1.9426
162	6.0000	64	12	0.1016	1.9426
194	6.0000	64	10	0.1016	1.9426
243	6.0000	64	8	0.1016	1.9426
260	6.0347	68	8	0.09502	2.0767
265	5.8876	52	6	0.1243	1.5881
275	6.0684	72	8	0.08974	2.1989
285	5.9266	56	6	0.1154	1.7103
290	6.1009	76	8	0.08502	2.3211
305	6.1326	80	8	0.08077	2.4432
324	6.0000	64	6	0.1016	1.9426
366	6.0684	72	6	0.08974	2.1989
397	5.8876	52	4	0.1243	1.5881
428	5.9266	56	4	0.1154	1.7103
458	5.9640	60	4	0.1077	1.8324
486	6.0000	64	4	0.1016	1.9426

$$U_\mu(x) \to g(x)U_\mu(x)g^\dagger(x + a\hat{e}_\mu), \quad g \in SU(3), \tag{4}$$

are physically equivalent and they define the gauge orbits. For the computation of the QCD Green's functions it is enough to consider one field from each orbit. The choice of a single configuration in the gauge orbits is known as gauge fixing.

In this work, we consider the minimal Landau gauge which, on the lattice, means maximizing, for each gauge configuration and on its orbit, the functional

$$F_U[g] = \frac{1}{4N_c V}\sum_x \sum_\mu \mathrm{Re}[\mathrm{Tr}(g(x)U_\mu(x)g^\dagger(x+\mu))], \tag{5}$$

where N_c the dimension of the gauge group and V the lattice volume. It can be shown, see, e.g., [128], that picking a maximum of $F_U[g]$ on a gauge orbit is equivalent to the usual continuum Landau gauge condition

$$\partial_\mu A_\mu^a = 0 \tag{6}$$

and implies also the positiveness of the Faddeev-Popov determinant.

In this work, the functional $F_U[g]$ was maximized using the Fourier accelerated steepest descent method as defined in [129]. The evolution and convergence of the gauge fixing process was monitored by

$$\theta = \frac{1}{N_c V}\sum_x \mathrm{Tr}[\Delta(x)\Delta^\dagger(x)], \tag{7}$$

where

$$\Delta(x) = \sum_\nu [U_\nu(x - a\hat{\nu}) - U_\nu(x) - \mathrm{H.c.} - \mathrm{trace}]. \tag{8}$$

The function $\Delta(x)$ is the lattice version of $\partial_\mu A_\mu$. The number θ gives the mean value of $\partial_\mu A_\mu = 0$ evaluated over all space-time lattice points per color degree of freedom. In all the results shown below, gauge fixing was stopped only when $\theta \leq 10^{-15}$. Gauge fixing was implemented using Chroma [127] and PFFT [130] libraries.

B. Gluon propagator definitions at finite T

In the Landau gauge and at finite temperature, the gluon propagator is described by two tensor structures,

$$D_{\mu\nu}^{ab}(p) = \langle A_\mu^a(p)A_\nu^b(-p)\rangle = \delta^{ab}\{P_{\mu\nu}^T D_T(p_4, \vec{p}) + P_{\mu\nu}^L D_L(p_4, \vec{p})\}, \tag{9}$$

where latin letters stand for color indices and greek letters for space-time indices. The transverse and longitudinal projectors are defined by

$$P^T_{\mu\nu} = (1-\delta_{\mu 4})(1-\delta_{\nu 4})\left(\delta_{\mu\nu} - \frac{p_\mu p_\nu}{\vec{p}^2}\right),$$
$$P^L_{\mu\nu} = \left(\delta_{\mu\nu} - \frac{p_\mu p_\nu}{p^2}\right) - P^T_{\mu\nu}. \quad (10)$$

The transverse and longitudinal form factors, respectively, D_T and D_L are given by

$$D_T(p) = \frac{1}{2V(N_c^2-1)}\left\{\langle A_i^a(p)A_i^a(-p)\rangle - \frac{p_4^2}{\vec{p}^2}\langle A_4^a(p)A_4^a(-p)\rangle\right\}$$
$$D_L(p) = \frac{1}{V(N_c^2-1)}\left(1+\frac{p_4^2}{p^2}\right)\langle A_4^a(p)A_4^a(-p)\rangle, \quad (11)$$

for $p \neq 0$, and

$$D_T(0) = \frac{1}{3V(N_c^2-1)}\langle A_i^a(0)A_i^a(0)\rangle \quad (12)$$

$$D_L(0) = \frac{1}{V(N_c^2-1)}\langle A_4^a(0)A_4^a(0)\rangle. \quad (13)$$

The momentum space gluon field $A_\mu^a(\tilde{p})$ reads

$$A_\mu(\tilde{p}) = \sum_x e^{-i\tilde{p}(x+\frac{a}{2}\hat{e}_\mu)}A_\mu(x+a\hat{e}_\mu/2), \quad (14)$$

$$A_\mu\left(x+\frac{a}{2}\hat{e}_\mu\right) = \frac{1}{2ig_0}[U_\mu(x)-U_\mu^\dagger] - \frac{1}{6ig_0}\mathrm{Tr}[U_\mu(x)-U_\mu^\dagger] \quad (15)$$

where

$$\tilde{p}_\mu = \frac{2\pi n_\mu}{aL_\mu}, \qquad n_\mu = 0,1,\ldots,L_\mu-1 \quad (16)$$

and L_μ is the lattice length over direction μ. For the continuum momentum we take the standard definition

$$q_\mu = \frac{2}{a}\sin\left(\frac{\pi}{L_\mu}n\right), \qquad n = 0,\ldots,L_\mu-1. \quad (17)$$

C. Renormalization of the lattice propagator

The lattice simulations summarized in Table I were performed using different lattice spacings but the same spatial volume $\sim(6.5\ \mathrm{fm})^3$. In order to compare the data coming from the different simulations, the lattice propagator was renormalized as described below.

The bare lattice form factors $D_T(q)$ and $D_L(q)$, after performing the momenta cuts discussed in Sec. II D, are fitted to the one-loop inspired result,

$$D(p^2) = \frac{Z}{p^2}\left(\ln\frac{p^2}{\Lambda^2}\right)^{-\gamma}, \quad (18)$$

where $\gamma = 13/22$ is the gluon anomalous dimension, including only the momenta $p \geq p_{\min}$, where $p_{\min}$ is the smallest momentum such that the χ^2/d.o.f. of fit to Eq. (18) is smaller than 1.8. Then, we use the fit results to compute the renormalization constant Z_R such that

$$D(p^2) = Z_R D_{\mathrm{Lat}}(p^2), \quad (19)$$

and requiring the renormalized propagator to verify

$$D(p^2)|_{p^2=\mu^2} = \frac{1}{\mu^2}. \quad (20)$$

For the renormalization scale we take $\mu = 4\ \mathrm{GeV} > p_{\min}$. All data shown below refer to renormalized form factors.

In what concerns renormalization, D_L and D_T were treated separately. It turned out that, for the same temperature, the Z_R associated with D_L and with D_T are compatible within one standard deviation.

D. Systematic effects

The simulations are performed on an hypercubic lattice which breaks rotational invariance. In order to reduce lattice spacing effects we have performed the cuts described in [10,131] for momenta above 1 GeV. For momenta below 1 GeV, we consider all the lattice data. In principle, the renormalization procedure with the momentum cuts removes all lattice spacing effects from lattice data. The results discussed in [16,18] corroborate this.

In the same set of papers, the longitudinal and transverse form factors show a moderate dependence on the lattice volume. Due to limited computational power, our strategy to minimize finite volume effects was to consider a fixed physical volume of $\sim(6.5\ \mathrm{fm})^3$. Given the large physical volume, we expect the finite volume effects to be small. For a discussion on the interplay between the finite volume and finite lattice spacing effects on the gluon propagator at zero temperature see [132].

At finite temperature and above T_c the center symmetry is spontaneously broken. Therefore, we expect a dependence of the gluon propagator on which $Z(3)$-sector the Polyakov loop belongs to [133]. To overcome this problem, in the simulations in the deconfined phase (where $P_L \neq 0$) a Z(3) flip with respect to the temporal direction was performed, such that the phase of the Polyakov loop average is in the interval $]-\pi/3,\pi/3]$.

Another source of systematics are Gribov copies, i.e., configurations which satisfy the Landau gauge condition but are related by finite gauge transformations. This is a difficult and very demanding computational problem for the lattice practitioner. However, the known SU(3) lattice simulations show that Gribov copies do not change

significantly the gluon propagator for the momenta considered here, i.e., that the effect due to the copies are, typically, within the statistical error; see, for example, [134,135]. Due to the limited computational power, in the present work we will not take into account possible effects due to Gribov copies.

III. GLUON PROPAGATOR AT FINITE T

The form factors $D_L(p^2)$ and $D_T(p^2)$, for $p_4 = 0$, as a function of the momentum $\vec{p}^2$ and temperature T are reported in Figs. 2 and 3. The zero momentum electric $D_T(0)$ and magnetic $D_L(0)$ form factors, as a function of T, can be seen in Fig. 4. Fig. 5 shows the ratio $D_L(p^2)/D_T(p^2)$ for the various temperatures which have been simulated (see Table I). Our results are in line with the simulations reported in Refs. [6,10,11,13].

The two gluon propagator form factors show quite different behaviors with T and p. The electric form factor $D_L(p^2)$ increases as one approaches the critical temperature from below and is strongly suppressed after T crosses T_c. This is clearly seen in the left upper plot of Fig. 2. For temperatures above the critical temperature $D_L(p^2)$ decreases monotonically as T takes higher values – see right upper plot in Fig. 2. Despite this drastic suppression of D_L as T increases, there is no obvious qualitative change of the function $D_L(p^2)$ with T and, for each T, the electric propagator is a decreasing function of the momentum.

On the other hand, the magnetic form factor $D_T(p^2)$ is clearly a monotonous decreasing function of T. Moreover, although D_T shows large changes with T, around $T_c \sim 270$ MeV it has the opposite behavior of D_L. Around T_c, the lower plots in Fig. 2 seem to indicate that the derivative essentially vanishes, increasing to $\partial D_T(p^2)/\partial T \sim 0$. Further, above T_c the functional form of $D_T(p^2)$ is different than for $T < T_c$. Indeed, above the critical temperature the magnetic propagator shows a turnover, with a maximum around $p \sim 500$ MeV, not seen in the lowest temperatures.

The different behavior of the form factors with T is illustrated in Fig. 4 for zero momentum. The figure shows that $D_L(0)$ and $D_T(0)$ are sensitive to the confinement-deconfinement transition. Furthermore, it also exhibits the relative order of magnitude of the electric and magnetic propagators which is detailed in Fig. 5. In the infrared region $D_L(p^2)$ is larger than $D_T(p^2)$ for the range of temperatures that we have accessed. However, for temperatures above ~ 360 MeV D_L and D_T have similar magnitudes close to zero momentum, with D_T becoming larger as p increases. For example, for the largest temperatures considered here, D_T is about 30% larger than D_L around

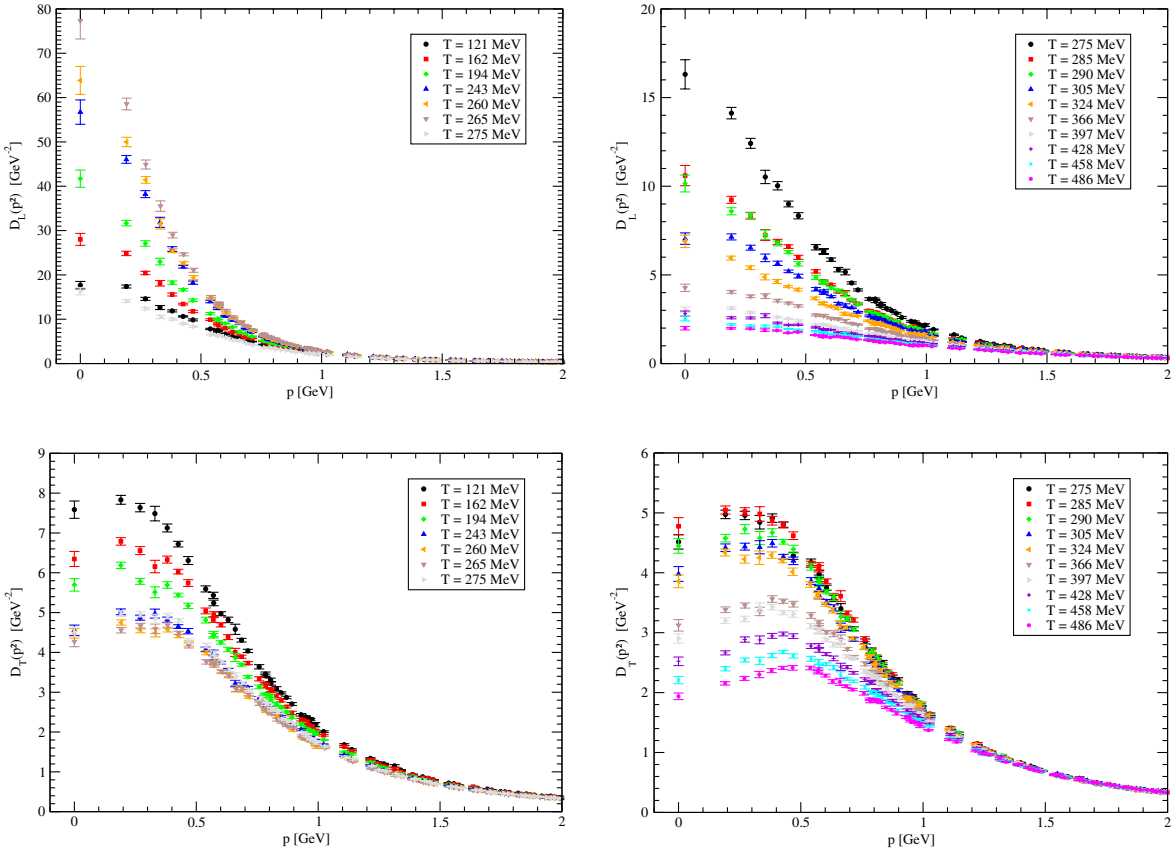

FIG. 2 (color online). Longitudinal (upper line) and transverse (lower line) gluon propagator form factors as a function of momentum p and temperature T for a $\sim(6.5\ \mathrm{fm})^3$ spatial lattice volume.

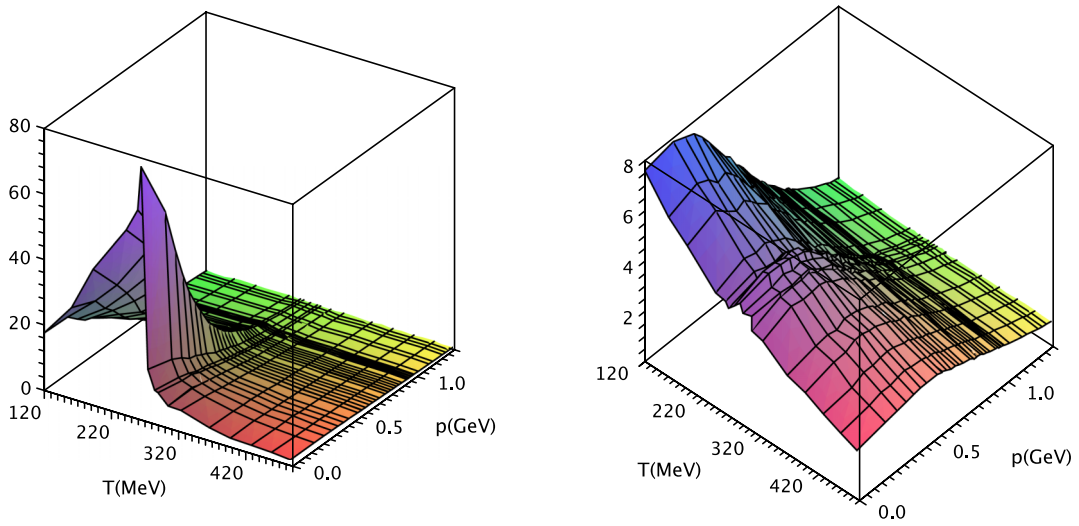

FIG. 3 (color online). Surface plots of the longitudinal (left figure) and transverse (right figure) gluon propagator form factors as a function of momentum p and temperature T.

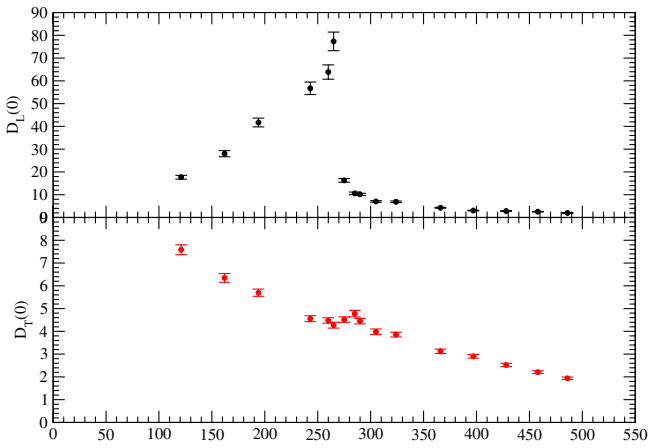

FIG. 4 (color online). Values of the electric and magnetic form factors at zero momentum, as a function of the temperature.

$p \sim 600$ MeV. At higher momenta D_L and D_T become identical for all T. This behavior for sufficiently high p is not unexpected, as the perturbative propagator should be recovered in the limit where $p \gg 1$.

IV. GLUON MASS AS A FUNCTION OF T

In this section, we consider different definitions for the electric and the magnetic gluon mass as a function of the temperature, extending the definitions in Refs. [12,43,111]. As discussed below, this will allow us to identify possible order parameters for the confinement-deconfinement phase transition.

A. Yukawa mass

In a quasiparticle description of the gluon as used, for example, in constituents models above T_c, the gluon is treated as a massive boson. In this picture, the propagator has a Yukawa form

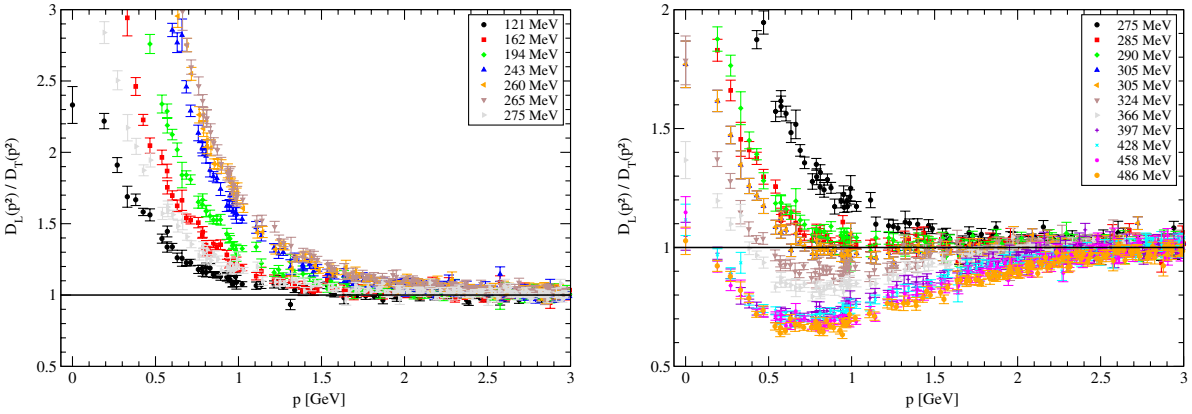

FIG. 5 (color online). $D_L(p^2)/D_T(p^2)$ as a function of the temperature.

$$D(p^2) = \frac{Z}{p^2 + m_g^2}, \tag{21}$$

where m_g is the gluon mass and $Z^{1/2}$ the overlap between the gluon state and the quasiparticle massive state.

The values for Z and m_g can be read from fitting the lattice data to (21) from $p = 0$ up to $p_{\max}$. The upper limit of the fitting interval should be determined in order to a have a $\chi^2/\text{d.o.f.} \sim 1$ and to ensure that the fitting parameters Z and m_g are independent of the upper bound of the fitting interval.

In general the gluon mass should be momentum dependent, $m_g = m_g(p^2, T)$, however if $m_g(p^2, T)$ is a slowly changing function of p^2, it is possible to identify an interval of momenta where $m_g(p^2, T)$ is constant and, in this way, define an infrared mass scale. For the gluon propagator at zero temperature such an analysis was performed in [39], where a $m_g = 648(7)$ MeV, a $Z = 4.044(78)$ for a $p_{\max} \sim 500$ MeV was found.

The magnetic propagator is clearly not described by a Yukawa type propagator for any of temperatures considered in this paper. Indeed, fitting the $D_T(p^2)$ lattice data to (21) always gives a $\chi^2/\text{d.o.f.}$ which is well above 2 for all the temperatures. We conclude that the magnetic propagator does not behave as a quasiparticle massive boson for the $T \lesssim 500$ MeV.

On the other hand the electric propagator is well described in the infrared region by a Yukawa propagator. In Fig. 6 we show how the fitting parameters and the quality of the fit, measured by the $\chi^2/\text{d.o.f.}$, changes with $p_{\max}$ for $T = 275$ MeV. Similar curves can be shown for the other temperatures.

The outcome of fitting the $D_L(p^2)$ lattice data to Eq. (21) are reported in Table II and are shown in Fig. 7. The curve in Fig. 7 is the fit of the measured gluon mass to the prediction of the perturbative [42] functional form of

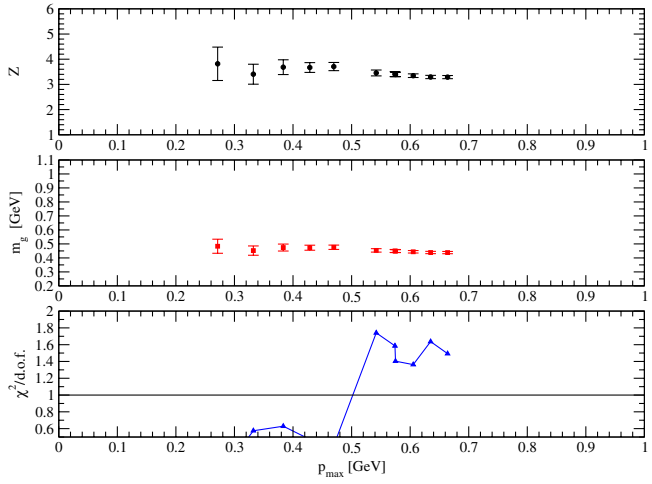

FIG. 6 (color online). Evolution of the fitting parameters with $p_{\max}$ for $T = 275$ MeV.

TABLE II. Results of fitting the longitudinal propagator $D_L(p^2)$ to the Yukawa (21) from $p = 0$ up to $p_{\max}$.

Temp. (MeV)	$p_{\max}$ (GeV)	Z	$m_g(T)$ (GeV)	$\chi^2/\text{d.o.f.}$
121	0.467	4.28(16)	0.468(13)	1.91
162	0.570	4.252(89)	0.3695(73)	1.66
194	0.330	5.84(50)	0.381(22)	0.72
243	0.330	8.07(67)	0.374(21)	0.27
260	0.271	8.73(86)	0.371(25)	0.03
265	0.332	7.34(45)	0.301(14)	1.03
275	0.635	3.294(65)	0.4386(83)	1.64
285	0.542	3.12(12)	0.548(16)	0.76
290	0.690	2.705(50)	0.5095(85)	1.40
305	0.606	2.737(80)	0.5900(32)	1.30
324	0.870	2.168(24)	0.5656(63)	1.36
366	0.716	2.242(55)	0.708(13)	1.80
397	0.896	2.058(34)	0.795(11)	1.03
428	1.112	1.927(24)	0.8220(89)	1.30
458	0.935	1.967(37)	0.905(13)	1.45
486	1.214	1.847(24)	0.9285(97)	1.55

Eq. (1), extended with a constant term to account for possible nonperturbative corrections,

$$m_g(T) = a + bT. \tag{22}$$

If one excludes the data point for $T = 428$ MeV, which seems to be slightly below the other data points for $m_g(T)$, Eq. (22) gives a good description of the gluon mass for $T \geq 397$ MeV. The measured parameters are $a = 193(88)$ MeV, $b = 1.52(20)$ for a $\chi^2/\text{d.o.f.} = 1.50$, where T and $m_g(T)$ are in MeV.

We would like to call the reader attention for the good agreement between $m_g = 0.32 \pm 0.07$ GeV estimated from experimental data for heavy ions [20] and our estimate for

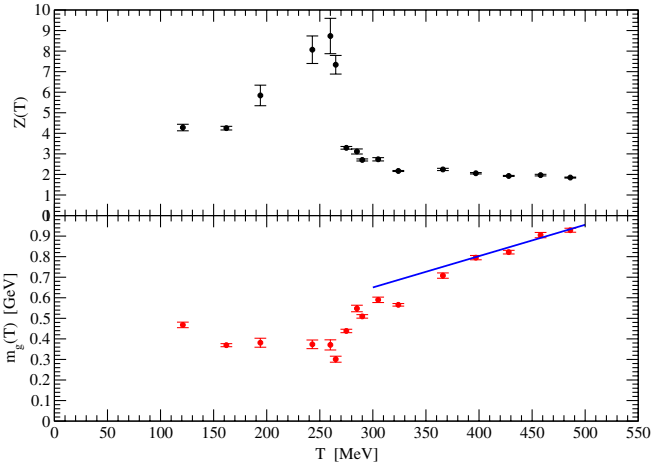

FIG. 7 (color online). $Z(T)$ and $m_g(T)$ from fitting the longitudinal gluon propagator to Eq. (21). The curve in the lower figure is the fit of m_g to the functional form predicted by the perturbation theory; see text for details.

$T = 265$ MeV where $m_g = 0.301 \pm 0.014$ GeV (see Table II).

We also call the reader's attention to the fact that in some earlier studies of gluon screening masses, such as [43,111], the propagator is computed in coordinate space, and a position space Yukawa form $G(z) = C\exp(-m_g z)$ is assumed. This is equivalent, in our approach, to consider (21) as an approximation to the gluon form factors. The masses are computed via the use of a point-to-all propagator and this procedure results in higher statistical errors. While the results of [43] are for Landau gauge but for the gauge group SU(2), [111] uses mainly the Feynman gauge and thus a direct comparison with our results should be done with care.

B. Running gluon mass

In [39] the zero temperature lattice gluon propagator for pure Yang-Mills SU(3) gauge theory was described via a running gluon mass which also describes the decoupling type of solution of the Dyson-Schwinger equations [37,38]. A generalized functional form for the running mass is able to described the gluon propagator over the full range of momenta and all T considered here.

Let us consider the following functional form for the gluon propagator

$$D(p^2) = \frac{Z(p^2;T)}{p^2 + M^2(p^2;T)}, \tag{23}$$

where

$$Z(p^2;T) = z_0\left[\ln\frac{p^2 + r(T)M^2(p^2;T)}{\Lambda^2(T)}\right]^{-\gamma}, \tag{24}$$

$\gamma = 13/22$ is the anomalous gluon dimension, and

$$M^2(p^2;T) = \frac{m_0^4(T)}{p^2 + m_1^2(T)} \tag{25}$$

is the temperature-dependent running gluon mass. Note that, if one takes $m_1 = m_0$ and ignores the temperature dependence, the above expression is the same functional form used in [39]. While in the $T \to 0$ limit it is sufficient [39] to consider a single massive parameter m_0, for the best fit at finite T we need to consider m_1 and m_0 as independent parameters.

The results of fitting the lattice longitudinal form factor to Eq. (23) are detailed in Table III. For all temperatures, $\chi^2/d.o.f.$ is close to unit; i.e., the functional form (23) is able to describe the lattice over the full range of momenta. The normalization $z_0 \sim 2$ is essentially independent of T. The temperature dependence of the various mass scales in (23) is summarized in Fig. 8. Of the mass scales Λ^2, m_0^2 and m_1^2 clearly Λ^2 is the most sensible to the confinement-deconfinement transition, taking the value $\Lambda \sim 0.89$ GeV for $T \lesssim T_c$ and $\Lambda \sim 0.67$ GeV for $T \gtrsim T_c$. In what concerns m_0^2 and m_1^2, the two mass scales are roughly constant up to $T \sim 300$ MeV, i.e., slightly above T_c, and increase with T for higher temperatures.

The functional form (23) allows for the definition of an infrared mass scale $m_g^{IR} = m_0^2/m_1$; note that for low momenta $p^2 \ll m_1^2$, (23) reduces to an Yukawa shape with a mass given by m^{IR}. $m_g^{IR}(T)$ can be seen in Fig. 9 and reproduces the same qualitative behavior as observed in the lower part of Fig. 7. Furthermore, we have checked that the temperature dependence of the data on Fig. 9 for $T > T_c$ is compatible with the perturbative inspired behavior resummed in Eq. (22). However, given the large statistical

TABLE III. Results of fitting the longitudinal propagator $D_L(p^2)$ to Eq. (23) for the range of momenta. The temperature is in MeV, while the mass scales are in powers of GeV.

T	z_0	r	Λ^2	m_0^4	m_1^2	$\chi^2/d.o.f$
121	1.9271(67)	11.5 ± 1.5	0.785(14)	0.078(14)	0.618(69)	1.28
162	1.9367(61)	11.7 ± 1.3	0.764(13)	0.066(10)	0.647(54)	1.18
194	1.9379(59)	14.2 ± 1.4	0.760(12)	0.0468(68)	0.599(45)	1.26
243	1.9237(57)	15.0 ± 1.4	0.789(12)	0.0415(54)	0.615(37)	1.47
260	1.9238(50)	19.7 ± 1.6	0.791(10)	0.0283(33)	0.530(29)	1.43
265	1.8847(65)	21.2 ± 1.8	0.857(13)	0.0321(39)	0.637(34)	1.45
275	2.0571(66)	11.9 ± 2.9	0.554(11)	0.051(15)	0.407(83)	1.12
285	2.105(12)	11.5 ± 5.2	0.478(17)	0.077(42)	0.47(19)	1.10
290	2.1224(59)	20.5 ± 7.7	0.4670(84)	0.040(16)	0.267(91)	1.06
305	2.1143(92)	4.6 ± 1.6	0.488(15)	0.280(95)	1.00(20)	1.10
324	2.141(15)	8.5 ± 5.3	0.447(21)	0.20(13)	0.79(39)	1.10
366	2.1684(73)	13.8 ± 4.5	0.4235(97)	0.187(57)	0.61(15)	0.96
397	2.138(34)	5.0 ± 4.8	0.453(50)	0.70(60)	1.42(83)	1.07
428	2.115(30)	4.2 ± 2.9	0.500(50)	1.12(68)	1.89(77)	1.00
458	2.168(13)	9.5 ± 4.3	0.436(17)	0.68(26)	1.24(37)	1.09
486	2.113(27)	2.9 ± 1.6	0.538(49)	2.32(95)	2.87(68)	1.03

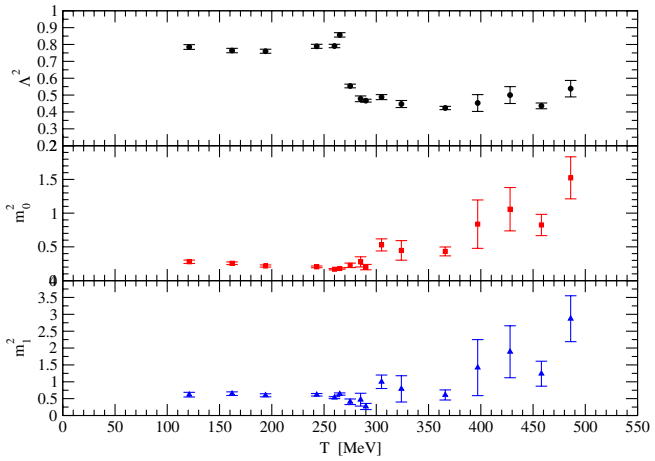

FIG. 8 (color online). Mass scales, in GeV^2, from fitting Eq. (23) to the lattice $D_L(p^2)$ over the full momentum range.

errors of the data, the estimated statistical errors on a and b are quite large (they are above 50%).

The functional form given in Eq. (23) is able to describe also the magnetic form factor $D_T(p^2)$. In Table IV we provide the output of the fits of the full range transverse lattice propagator data for the various temperatures. Again, the overall normalization factor $z_0 \sim 2$ seems to be independent of T. Λ shows a nonmonotonic behavior with T, while m_0^2 and m_1^2 are increasing functions of T. However, the mass scales $\Lambda^2(T)$, $m_0^2(T)$ and $m_1^2(T)$ do not show a clear indication of the confinement-deconfinement phase transition.

Similarly to the electric form factor, one can define an infrared mass scale associated with the magnetic form factor as $m_g^{IR} = m_0^2/m_1$; see Fig. 10 for details on the fits. This mass scale, as a function of the temperature, is shown in Fig. 11. The figure points to $m_g^{IR}(T)$ as a linear function of T. Indeed, a linear fit (full line seen in Fig. 11) to the $m_g^{IR}(T)$ gives

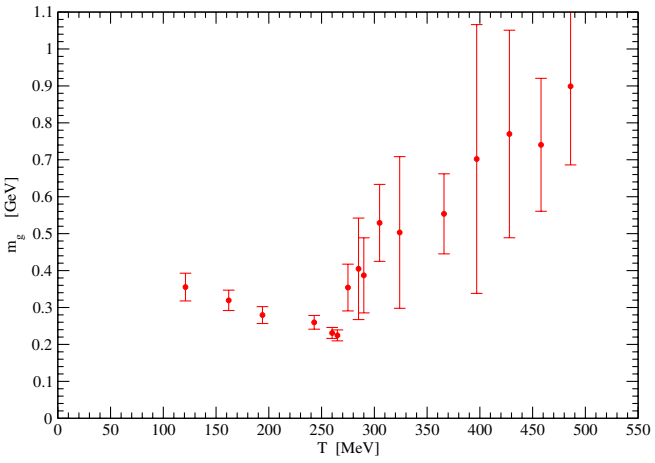

FIG. 9 (color online). Infrared mass scale associated with $D_L(p^2)$ taken as m_0^2/m_1.

$$m_g^{IR}(T) = (303.0 \pm 8.1) + (0.989 \pm 0.025)T \qquad (26)$$

for a $\chi^2/\text{d.o.f.} = 0.05$ with all dimensionful quantities given in MeV.

A linear behavior of the magnetic screening mass m_{mag} has been used in the perturbative approach to hot QCD; see, e.g., [4,27,136] and references therein. Furthermore, as already stated in the introduction, the perturbative approach to QCD assumes that the Debye screening mass associated with the electric form factor is such that, in leading order, $m_D \sim gT$, while the magnetic mass needed to regulate the perturbative expansion goes as $m_{\text{mag}} \sim g^2 T$. In this sense, our results validate, within the statistical accuracy of the simulations, the functional dependence of the m_D and m_{mag} as taken in perturbation theory.

C. Zero momentum mass scale

The infrared mass scale $m_D(T)$ associated with the electric form factor $D_L(p^2;T)$ show quite a different behavior below and above T_c (see Figs. 7 and 9). Indeed, $m_D(T)$ can be used as an order parameter for the confinement-deconfinement phase transition. On the other hand, the infrared mass scale $m_{\text{mag}}(T)$, linked with the magnetic form factor $D_T(p^2;T)$, shows a monotonous behavior with T, see Fig. 11, and it is not obvious that it can be used to identify the phase transition.

The definitions of m_D or m_{mag} considered in the previous section requires fitting the lattice data to a given functional form either (21) or (23). Alternatively, one can use directly the lattice propagator data to define a nonperturbative mass scale. A possible choice is to connect the mass scale with the deep infrared propagator, as in Refs. [12,43]. So let us consider

$$m(T) = 1/\sqrt{D(p^2 = 0;T)}, \qquad (27)$$

as used in [12]. This choice is equivalent to a Yukawa fit of Eq. (21) setting the parameter $Z = 1$, as used, e.g., for the high-T region [43].

The comparison of our data with [12] requires choosing a different renormalization scale, namely $\mu = 2$ GeV. The two sets of data for the electric form factor $D_L(p^2;T)$, i.e., taking $m = 1/\sqrt{D_L(0)}$, are compared in Fig. 12 and show essentially the same type of dependence with T/T_c.

The differences between the two sets of data in Fig. 12 are possibly due to the finite volume effects and the lattice spacing effects. While the simulations reported here are performed considering a spatial volume $V_s \approx (6.5\ \text{fm})^3$ and lattice spacings smaller than 0.12 fm, those in [12] used spatial volumes between $(2.92 - 7.49\ \text{fm})^3$ and lattice spacings larger than 0.16 fm. While our smallest β value is 5.8876, [12] used $\beta \in [5.642, 5.738]$. Furthermore, to build Fig. 12 we take $T_c = 270$ MeV when using our data, while [12] uses $T_c = 277$ MeV. Given that we do not cover

TABLE IV. Results of fitting the transverse propagator $D_T(p^2)$ to Eq. (23) for the range of momenta. The temperature is in MeV, while the mass scales are in powers of GeV.

T	z_0	r	Λ^2	m_0^4	m_1^2	χ^2/d.o.f.
121	1.9723(41)	26.8 ± 3.8	0.6922(73)	0.0261(39)	0.143(20)	1.72
162	2.0067(49)	20.8 ± 3.1	0.6313(79)	0.0356(54)	0.164(23)	1.89
194	2.0468(44)	14.7 ± 2.1	0.5671(67)	0.0535(73)	0.215(25)	1.34
243	2.1211(52)	11.1 ± 1.7	0.4614(66)	0.0724(97)	0.236(27)	1.41
260	2.1547(54)	9.8 ± 1.7	0.4210(66)	0.085(12)	0.262(32)	1.56
265	2.1567(66)	11.0 ± 1.6	0.4101(72)	0.0734(87)	0.228(24)	1.31
275	2.1408(46)	10.2 ± 1.5	0.4379(59)	0.0718(92)	0.230(25)	1.36
285	2.1359(56)	9.1 ± 1.6	0.4375(66)	0.077(12)	0.247(31)	1.29
290	2.1597(41)	7.6 ± 1.3	0.4194(51)	0.090(12)	0.257(29)	1.17
305	2.1553(41)	8.8 ± 1.3	0.4241(54)	0.088(11)	0.249(26)	1.26
324	2.1617(52)	6.6 ± 1.3	0.4113(60)	0.110(17)	0.286(34)	1.32
366	2.1505(50)	7.0 ± 1.2	0.4308(64)	0.134(17)	0.293(31)	1.42
397	2.1110(67)	7.6 ± 1.2	0.4693(83)	0.142(17)	0.302(29)	1.36
428	2.0921(65)	8.6 ± 1.1	0.5014(89)	0.156(15)	0.299(24)	1.45
458	2.0860(61)	7.2 ± 1.0	0.5150(86)	0.205(21)	0.345(29)	1.41
496	2.0629(60)	8.7 ± 1.0	0.5543(93)	0.210(18)	0.330(24)	1.54

the transition region with great detail, this difference on the transition temperature does not change drastically the outcome of Fig. 12.

The electric and magnetic masses defined with Eq. (27) are compared in Fig. 13 and reproduce the behavior observed in Figs. 7, 9, and 11. In Ref. [43] the large T limit was studied. The authors have shown that the magnetic mass is eventually suppressed, $m_D/m_{\mathrm{mag}} \sim \log T$. Here we find the magnetic mass m_{mag} is larger that the Debye mass when $T < 2T_c$. Only at $T \sim 2T_c$ the electric mass m_D takes over the magnetic mass and, therefore, it is only for $T \gtrsim 2T_c$ that the transverse degrees of freedom become dominant. Thus, for the temperatures considered here, $T \in [0, 2T_c]$, the low-temperature degrees of freedom associated with the gluon longitudinal degrees of freedom are still relevant, and the perturbative magnetic gluon gas does not completely set in yet.

Note that at $T = T_c = 270$ MeV, the electric mass m_D reaches its minimum value. Given that we do not cover the transition region with great detail, it is not clear from our data whether the mass is discontinuous or its derivative is discontinuous. Nevertheless, when T crosses T_c, our data for the electric mass m_D is consistent with a phase transition.

V. SUMMARY AND CONCLUSIONS

We have computed the gluon propagator at finite temperature using lattice QCD simulations for pure gauge SU(3) Yang-Mills theory on a large spatial volume $V_s \approx (6.5\ \mathrm{fm})^3$. Our results are similar to those found by different authors [6,10,11,13].

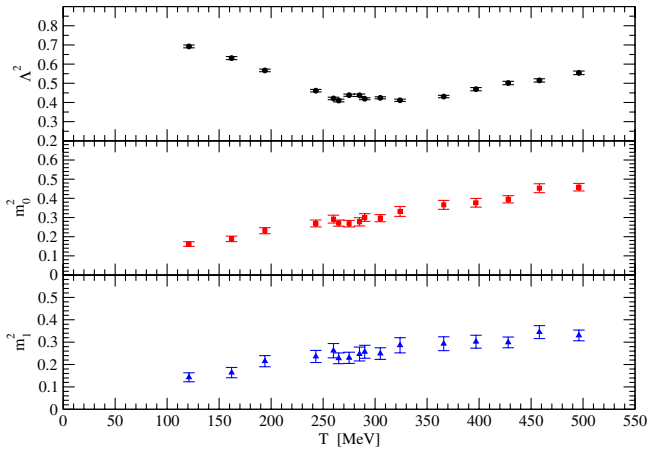

FIG. 10 (color online). Mass scales, in GeV^2, from fitting Eq. (23) to the lattice $D_T(p^2)$ over the full momentum range.

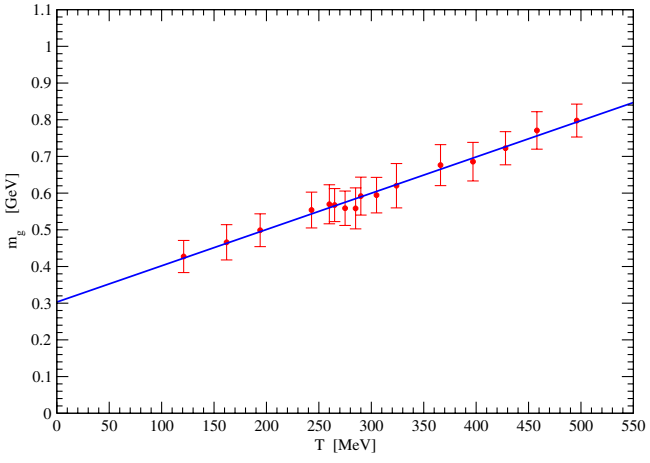

FIG. 11 (color online). Infrared mass scale associated with $D_T(p^2)$ taken as m_0^2/m_1. The full line is the outcome of the linear fit described in the text [see Eq. (26)].

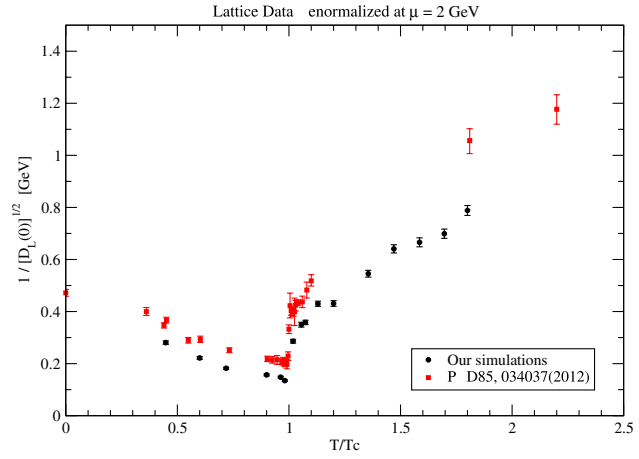

FIG. 12 (color online). Electric mass defined by Eq. (27) for the simulations reported in Table I renormalized at $\mu = 2$ GeV compared with the data of [12].

The electric form factor $D_L(p^2;T)$ and the magnetic form factor $D_T(p^2;T)$ have different behaviors as one crosses the confinement-deconfinement phase transition temperature $T_c \approx 270$ MeV. For $T < T_c$, $D_L(p^2;T)$ increases with T and is larger than $D_T(p^2;T)$. For $T > T_c$, $D_L(p^2;T)$ decreases with T and becomes of the same order of magnitude of $D_T(p^2;T)$ for $T \sim 400$ MeV. The exact value of the ratio $D_L(p^2;T)/D_T(p^2;T)$ depends, for each T, on the value of p^2. The magnetic form factor $D_T(p^2;T)$ is a decreasing function of T for all the temperatures considered here. However, its nature changes when $T > T_c$ and one observe a turnover with $D_T(p^2;T)$ having a maximum just below $p \sim 500$ MeV. Note, however, that the data in Fig. 2 do not exclude completely a temperature dependent shift of the turnover for the magnetic form factor, instead of a functional change of $D_T(p^2;T)$ as T crosses the deconfinement phase transition. Indeed, if one assumes that the temperature only induces a shift in the turnover of $D_T(p^2;T)$, then for $T < T_c$ the turnover should happen for very low momenta $p \sim 200 - 300$ MeV. Our simulation do not access momenta below ~ 200 MeV, with the exception of $p = 0$ MeV, and we are unable to distinguish the two scenarios.

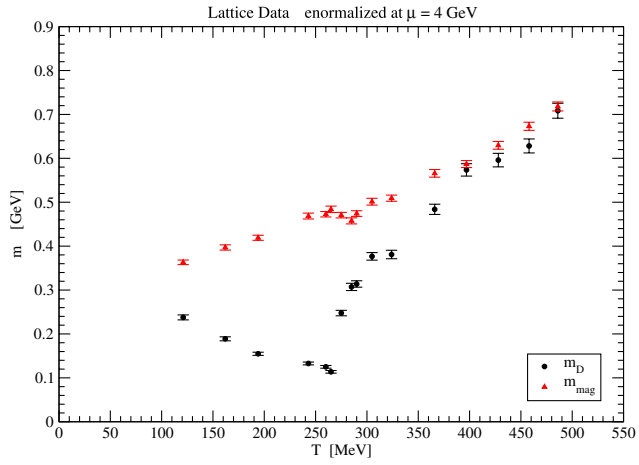

FIG. 13 (color online). Electric and magnetic mass defined by Eq. (27) for the simulations reported in Table I.

For low momenta, we investigated the interpretation of the gluon form factors in terms of a quasiparticle Yukawa-like propagator, extracting the gluon screening mass $m(T)$ as a function of the temperature T. We continued previous lattice QCD studies of the gluon screening mass in Landau gauge. Many years ago, in Ref. [43], the screening electric and magnetic gluon masses were studied, for the first time, for the gauge group $SU(2)$ and reaching temperatures as high as $10^4 T_c$. The authors found good agreement with finite temperature field theory. Since this impressive [43] temperature range $2T_c < T < 10^4 T_c$, lattice QCD studies started to focus in temperatures closer to the deconfinement region. Ref. [111] studied $SU(3)$ gluodynamics in covariant gauges (mainly Feynman gauge) using stochastic gauge fixing, exploring with a greater detail temperatures closer to the transition temperature T_c and going only up to $16T_c$. A finite value for the screening mass in the confinement region, i.e., for $T < T_c$, was not measured. This is probably due to the method used to extract the mass, which relies on a point-to-all propagator; furthermore, the gluon mass for SU(3) is for the Feynman gauge. The authors of [111] only concluded that the confining screening mass was very large and possibly infinite. Recently, Ref. [12] was able to explore larger volumes and found finite screening masses both above and below T_c. In particular, the authors found a finite screening mass $m_D(T)$ in the range $0 < T < 3T_c$ and they covered in great detail the transition region of $T \sim T_c$. Notice a finite mass, for $T \sim 0$, is consistent with the recent study of Ref. [39]. In the present work, we used for all temperatures $0 < T < 2T_c$ the same large lattice volume of $(6.5\ \mathrm{fm})^3$. Our propagators are compatible with the ones of Ref. [12], and thus we confirm finite gluon masses for all values of T, including the confining sector of gluodynamics. Note that the screening mass was measured in Refs. [12,43] looking only to the lowest momentum $p \sim 0$ of the gluon propagators. Here we explored the gluon propagator form factors $D_L(p^2;T)$ and $D_T(p^2;T)$ in a wider momentum region, which allow us to explore different possible definitions of the gluon screening mass.

Whereas the infrared $D_L(p^2;T)$ can be described by a quasiparticle Yukawa-like propagator for all the simulated temperatures, the low momenta magnetic form factor $D_T(p^2;T)$ is not compatible with such a simple interpretation of the propagator.

The interpretation of the low momenta $D_L(p^2;T)$ in terms of a massive Yukawa-like propagator provides a definition of a temperature dependent longitudinal gluon screening mass $m_D(T)$. Furthermore, this simple picture defines also an "overlap" of the gluon state with a massive

quasiparticle boson state associated with $Z(T)$. It follows that $m_D(T)$ and $Z(T)$ are sensitive to the confinement-deconfinement phase transition. The data for $m_D(T)$ suggests that the deconfinement phase transition be of first order.

We observe that $m_D(T)$ is a decreasing function of T for $T < T_c$, and is an increasing function of T above the confinement-deconfinement phase transition. Moreover, the gluon mass follows the expected perturbative functional dependence starting at temperatures as low as $T \sim 400$ MeV.

Besides the Yukawa approximation to the longitudinal propagator, we also consider the case of a temperature dependence running gluon mass which is motivated by the nonperturbative decoupling solution of the Dyson-Schwinger equations and that is able to describe the lattice data at $T = 0$. The functional form, which takes into account logarithmic corrections as suggested by perturbative QCD, is able to describe quite well both the longitudinal and transverse gluon form factors for all the temperatures and over the full range of momenta. Moreover, it allows a definition of infrared mass scales m^{IR} associated with $D_L(p^2;T)$ and $D_T(p^2;T)$. In what concerns the longitudinal form factor $D_L(p^2;T)$ the corresponding $m^{IR}(T)$ reproduces, with large statistical errors, the behavior of the gluon mass taken from the Yukawa fit. On the other hand, the magnetic $m^{IR}(T)$ is compatible with a linear behavior with T over the full range of temperatures simulated. This linear behavior above T_c is in good agreement with the perturbative approach to hot QCD.

Last but not least, we consider a mass scale taken directly from the longitudinal gluon propagator data at zero momentum $1/\sqrt{D_L(0)}$ as investigated in [12]. In this way, we avoid modeling the propagator. This mass scale reproduces the same pattern as observed for the mass taken from the Yukawa or the running mass fits. Any of the definitions can be used as order parameter to identify the confinement-deconfinement phase transition.

As an outlook of our research, with more computer power, it would be useful to further increase the lattice volume while decreasing the lattice spacing, in order to be able to extrapolate to the continuum limit. It will also be relevant to scan in more detail the transition region, which would open the possibility to investigate a possible splitting of the gluon mass [137–139].

ACKNOWLEDGMENTS

The authors acknowledge the Laboratory for Advanced Computing at the University of Coimbra for providing HPC computing resources that have contributed to the research results reported within this paper (http://www.lca.uc.pt). P. J. Silva acknowledges support by F. C. T. under Contract No. SFRH/BPD/40998/2007. This work was supported by Projects No. CERN/FP/123612/2011, No. CERN/FP/123620/2011, and No. PTDC/FIS/100968/2008, projects developed under initiative QREN financed by UE/FEDER through the program COMPETE. We thank the authors of [12] for sending us the data reported in Fig. 12.

[1] J. Fingberg, U. M. Heller, and F. Karsch, Nucl. Phys. **B392**, 493 (1993).
[2] B. Lucini, M. Teper, and U. Wenger, J. High Energy Phys. 01 (2004) 061.
[3] A. V. Smilga, Phys. Rep. **291**, 1 (1997).
[4] J. O. Andersen and M. Strickland, Ann. Phys. (Amsterdam) **317**, 281 (2005).
[5] A. Cucchieri, A. Maas, and T. Mendes, Phys. Rev. D **75**, 076003 (2007).
[6] C. S. Fischer, A. Maas, and J. A. Muller, Eur. Phys. J. C **68**, 165 (2010).
[7] V. Bornyakov and V. Mitrjushkin, Phys. Rev. D **84**, 094503 (2011).
[8] A. Cucchieri and T. Mendes, *Proc. Sci.*, LATTICE2010 (**2010**) 280.
[9] V. Bornyakov and V. Mitrjushkin, Int. J. Mod. Phys. A **27**, 1250050 (2012).
[10] R. Aouane, V. G. Bornyakov, E.-M. Ilgenfritz, V. K. Mitrjushkin, M. Müller-Preussker, and A. Sternbeck, Phys. Rev. D **85**, 034501 (2012).
[11] A. Cucchieri and T. Mendes, *Proc. Sci.*, FACESQCD2010 (**2010**) 007.
[12] A. Maas, J. M. Pawlowski, L. von Smekal, and D. Spielmann, Phys. Rev. D **85**, 034037 (2012).
[13] A. Cucchieri and T. Mendes, *Proc. Sci.*, LATTICE2011 (**2011**) 206.
[14] A. Maas, Phys. Rep. **524**, 203 (2013).
[15] A. Cucchieri, D. Dudal, T. Mendes, and N. Vandersickel, arXiv:1202.0639.
[16] O. Oliveira and P. J. Silva, Acta Phys. Pol. B Proc. Suppl. **5**, 1039 (2012).
[17] O. Oliveira and P. Silva, *Proc. Sci.*, LATTICE2012 (**2012**) 216.
[18] P. J. Silva and O. Oliveira, *Proc. Sci.*, Confinement X (**2012**) 045.
[19] P. Costa, O. Oliveira, and P. Silva, Phys. Lett. B **695**, 454 (2011).
[20] P. Bicudo, F. Giacosa, and E. Seel, Phys. Rev. C **86**, 034907 (2012).
[21] E. V. Shuryak, Sov. Phys. JETP **47**, 212 (1978).
[22] D. J. Gross, R. D. Pisarski, and L. G. Yaffe, Rev. Mod. Phys. **53**, 43 (1981).
[23] N. Weiss, Phys. Rev. D **25**, 2667 (1982).
[24] T. Toimela, Z. Phys. C **27**, 289 (1985).

[25] T. Furusawa and K. Kikkawa, Phys. Lett. **128B**, 218 (1983).
[26] E. Braaten and R. D. Pisarski, Phys. Rev. D **45**, R1827 (1992).
[27] A. Rebhan, arXiv:hep-ph/9310202.
[28] K. Amemiya and H. Suganuma, Phys. Rev. D **60**, 114509 (1999).
[29] A. Aguilar, A. Natale, and P. R. da Silva, Phys. Rev. Lett. **90**, 152001 (2003).
[30] D. Dudal, H. Verschelde, J. Gracey, V. Lemes, and M. Sarandy, J. High Energy Phys. 01 (2004) 044.
[31] K.-I. Kondo, A. Ono, A. Shibata, T. Shinohara, and T. Murakami, J. Phys. A **39**, 13767 (2006).
[32] K.-I. Kondo, Phys. Rev. D **74**, 125003 (2006).
[33] D. Dudal, M. A. L. Capri, J. A. Gracey, V. E. R. Lemes, R. F. Sobreiro, S. P. Sorella, and H. Verschelde, Nucl. Phys. B, Proc. Suppl. **174**, 201 (2007).
[34] F. Ford and J. Gracey, Phys. Lett. B **674**, 232 (2009).
[35] A. Cucchieri, D. Dudal, T. Mendes, and N. Vandersickel, Phys. Rev. D **85**, 094513 (2012).
[36] S. Gongyo, T. Iritani, and H. Suganuma, Phys. Rev. D **86**, 094018 (2012).
[37] J. M. Cornwall, Phys. Rev. D **26**, 1453 (1982).
[38] A. Aguilar, D. Binosi, and J. Papavassiliou, Phys. Rev. D **78**, 025010 (2008).
[39] O. Oliveira and P. Bicudo, J. Phys. G **38**, 045003 (2011).
[40] J. Kapusta and C. Gale "Finite-temperature field theory: principles and applications", CUP (2006).
[41] Z. Xu and C. Greiner, Phys. Rev. C **79**, 014904 (2009).
[42] P. B. Arnold and L. G. Yaffe, Phys. Rev. D **52**, 7208 (1995).
[43] U. M. Heller, F. Karsch, and J. Rank, Phys. Rev. D **57**, 1438 (1998).
[44] A. Nakamura and T. Saito, Prog. Theor. Phys. **111**, 733 (2004).
[45] P. Petreczky and K. Petrov, Phys. Rev. D **70**, 054503 (2004).
[46] F. Karsch, J. Phys. G **30**, S887 (2004).
[47] O. Kaczmarek and F. Zantow, *Proc. Sci.*, LAT2005 (**2005**) 192.
[48] O. Kaczmarek and F. Zantow, arXiv:hep-lat/0506019.
[49] O. Kaczmarek and F. Zantow, Phys. Rev. D **71**, 114510 (2005).
[50] K. Huebner, F. Karsch, O. Kaczmarek, and O. Vogt, Phys. Rev. D **77**, 074504 (2008).
[51] M. Doring, K. Huebner, O. Kaczmarek, and F. Karsch, Phys. Rev. D **75**, 054504 (2007).
[52] P. Bicudo, M. Cardoso, P. Santos, and J. Seixas, arXiv:0804.4225.
[53] P. Bicudo, J. Seixas, and M. Cardoso, arXiv:0906.2676.
[54] W. Greiner and D. Rischke, Phys. Rep. **264**, 183 (1996).
[55] J. Burdanov and G. Efimov, Phys. Rev. D **64**, 014001 (2001).
[56] D. Jia, arXiv:hep-th/0509030.
[57] T. Suzuki, K. Ishiguro, Y. Mori, and T. Sekido, AIP Conf. Proc. **756**, 172 (2005).
[58] H. Suganuma, K. Amemiya, H. Ichie, and Y. Koma, arXiv:hep-ph/0407121.
[59] H. Suganuma *et al.*, arXiv:hep-lat/0407020.
[60] H. Suganuma and H. Ichie, Nucl. Phys. B, Proc. Suppl. **121**, 316 (2003).
[61] A. Kumar and R. Parthasarathy, Phys. Lett. B **595**, 373 (2004).
[62] N. Cardoso, M. Cardoso, and P. Bicudo, arXiv:1004.0166.
[63] M. S. Cardaci, P. Cea, L. Cosmai, R. Falcone, and A. Papa, Phys. Rev. D **83**, 014502 (2011).
[64] P. Cea, L. Cosmai, and A. Papa, Phys. Rev. D **86**, 054501 (2012).
[65] V. Mathieu, C. Semay, and F. Brau, Eur. Phys. J. A **27**, 225 (2006).
[66] V. Mathieu, C. Semay, and B. Silvestre-Brac, Phys. Rev. D **74**, 054002 (2006).
[67] V. Mathieu, F. Buisseret, and C. Semay, Phys. Rev. D **77**, 114022 (2008).
[68] V. Mathieu, C. Semay, and B. Silvestre-Brac, Phys. Rev. D **77**, 094009 (2008).
[69] N. Boulanger, F. Buisseret, V. Mathieu, and C. Semay, Eur. Phys. J. A **38**, 317 (2008).
[70] V. Mathieu, N. Kochelev, and V. Vento, Int. J. Mod. Phys. E **18**, 1 (2009).
[71] V. Mathieu, F. Buisseret, C. Semay, and B. Silvestre-Brac, arXiv:0811.2710.
[72] F. Buisseret, V. Mathieu, and C. Semay, Phys. Rev. D **80**, 074021 (2009).
[73] V. Mathieu and V. Vento, Phys. Rev. D **81**, 034004 (2010).
[74] V. Mathieu, Acta Phys. Pol. B Proc. Suppl. **4**, 677 (2011).
[75] A. Szczepaniak, E. S. Swanson, C.-R. Ji, and S. R. Cotanch, Phys. Rev. Lett. **76**, 2011 (1996).
[76] F. J. Llanes-Estrada, S. R. Cotanch, P. J. de A. Bicudo, J. E. F. T. Ribeiro, and A. P. Szczepaniak, Nucl. Phys. **A710**, 45 (2002).
[77] F. J. Llanes-Estrada, P. Bicudo, and S. R. Cotanch, Phys. Rev. Lett. **96**, 081601 (2006).
[78] P. Bicudo, S. R. Cotanch, F. J. Llanes-Estrada, and D. G. Robertson, Eur. Phys. J. C **52**, 363 (2007).
[79] W.-S. Hou, C.-S. Luo, and G.-G. Wong, Phys. Rev. D **64**, 014028 (2001).
[80] W.-S. Hou and G.-G. Wong, Phys. Rev. D **67**, 034003 (2003).
[81] K. Ishikawa, M. Teper, and G. Schierholz, Phys. Lett. B **116**, 429 (1982).
[82] K. Ishikawa, M. Teper, and G. Schierholz, Phys. Lett. B **110**, 399 (1982).
[83] K. Ishikawa, G. Schierholz, and M. Teper, Z. Phys. C **16**, 69 (1982).
[84] K. Ishikawa, G. Schierholz, H. Schneider, and M. Teper, Nucl. Phys. **B227**, 221 (1983).
[85] K. Ishikawa, G. Schierholz, and M. Teper, Z. Phys. C **19**, 327 (1983).
[86] K. Ishikawa, A. Sato, G. Schierholz, and M. Teper, Z. Phys. C **21**, 167 (1983).
[87] G. Schierholz and M. Teper, Phys. Lett. **136B**, 64 (1984).
[88] P. de Forcrand, G. Schierholz, H. Schneider, and M. Teper, Phys. Lett. **152B**, 107 (1985).
[89] P. de Forcrand, G. Schierholz, H. Schneider, and M. Teper, Z. Phys. C **31**, 87 (1986).
[90] B. Carpenter, C. Michael, and M. Teper, Phys. Lett. B **198**, 511 (1987).
[91] M. Teper, Phys. Lett. B **183**, 345 (1987).
[92] C. Michael and M. Teper, Phys. Lett. B **206**, 299 (1988).
[93] M. Teper, Phys. Lett. B **185**, 121 (1987).

[94] C. Michael, G. Tickle, and M. Teper, Phys. Lett. B **207**, 313 (1988).
[95] C. Michael and M. Teper, Nucl. Phys. **B314**, 347 (1989).
[96] M. J. Teper, Phys. Rev. D **59**, 014512 (1998).
[97] P. Stephenson and M. Teper, Nucl. Phys. **B327**, 307 (1989).
[98] K. M. Bitar, R. Edwards, U. M. Heller, A. Kennedy, T. A. DeGrand *et al.*, Phys. Rev. D **44**, 2090 (1991).
[99] J. Kogut, D. Sinclair, and M. Teper, Phys. Rev. D **44**, 2869 (1991).
[100] T. Moretto and M. Teper, arXiv:hep-lat/9312035.
[101] R. W. Johnson and M. J. Teper, Phys. Rev. D **66**, 036006 (2002).
[102] A. Hart and M. Teper (UKQCD Collaboration), Phys. Rev. D **65**, 034502 (2002).
[103] H. B. Meyer and M. J. Teper, Nucl. Phys. **B658**, 113 (2003).
[104] H. B. Meyer and M. J. Teper, Nucl. Phys. **B668**, 111 (2003).
[105] B. Lucini, M. Teper, and U. Wenger, J. High Energy Phys. 06 (2004) 012.
[106] H. B. Meyer and M. J. Teper, Phys. Lett. B **605**, 344 (2005).
[107] C. J. Morningstar and M. J. Peardon, Phys. Rev. D **56**, 4043 (1997).
[108] C. J. Morningstar and M. J. Peardon, Phys. Rev. D **60**, 034509 (1999).
[109] Y. Chen, A. Alexandru, S. Dong, T. Draper, I. Horvath *et al.*, Phys. Rev. D **73**, 014516 (2006).
[110] A. Aguilar, D. Ibanez, V. Mathieu, and J. Papavassiliou, Phys. Rev. D **85**, 014018 (2012).
[111] A. Nakamura, T. Saito, and S. Sakai, Phys. Rev. D **69**, 014506 (2004).
[112] O. Oliveira, D. Dudal, and P. Silva, *Proc. Sci.*, LATTICE2012 (**2012**) 214.
[113] D. Dudal, P. J. Silva, and O. Oliveira, *Proc. Sci.*, Confinement X (**2012**) 033.
[114] D. Dudal, O. Oliveira, and P. J. Silva, Phys. Rev. D **89**, 014010 (2014).
[115] R. Karplus, C. M. Sommerfield, and E. H. Wichmann, Phys. Rev. **111**, 1187 (1958).
[116] L. Landau, Nucl. Phys. **13**, 181 (1959).
[117] R. Cutkosky, J. Math. Phys. (N.Y.) **1**, 429 (1960).
[118] C. S. Fischer and R. Williams, Phys. Rev. Lett. **103**, 122001 (2009).
[119] D. Dudal and M. S. Guimaraes, Phys. Rev. D **83**, 045013 (2011).
[120] A. Windisch, R. Alkofer, G. Haase, and M. Liebmann, Comput. Phys. Commun. **184**, 109 (2013).
[121] A. Windisch, M. Q. Huber, and R. Alkofer, Phys. Rev. D **87**, 065005 (2013).
[122] S. Strauss, C. S. Fischer, and C. Kellermann, Phys. Rev. Lett. **109**, 252001 (2012).
[123] A. Windisch, M. Q. Huber, and R. Alkofer, *Proc. Sci.*, Confinement X (**2012**) 060.
[124] A. Windisch, M. Q. Huber, and R. Alkofer, Acta Phys. Pol. B Proc. Suppl. **6**, 887 (2013).
[125] G. S. Bali and K. Schilling, Phys. Rev. D **47**, 661 (1993).
[126] S. Necco and R. Sommer, Nucl. Phys. **B622**, 328 (2002).
[127] R. G. Edwards and B. Joo (SciDAC Collaboration, LHPC Collaboration, UKQCD Collaboration), Nucl. Phys. B, Proc. Suppl. **140**, 832 (2005).
[128] O. Oliveira and P. Silva, Comput. Phys. Commun. **158**, 73 (2004).
[129] C. Davies, G. Batrouni, G. Katz, A. Kronfeld, G. Lepage, K. Wilson, P. Rossi, and B. Svetitsky, Phys. Rev. D **37**, 1581 (1988).
[130] M. Pippig, SIAM J. Sci. Comput. **35**, C213 (2013).
[131] D. B. Leinweber, J. I. Skullerud, A. G. Williams, and C. Parrinello (UKQCD), Phys. Rev. D **60**, 094507 (1999).
[132] O. Oliveira and P. J. Silva, Phys. Rev. D **86**, 114513 (2012).
[133] G. Damm, W. Kerler, and V. Mitrjushkin, Phys. Lett. B **433**, 88 (1998).
[134] P. J. Silva and O. Oliveira, Nucl. Phys. **B690**, 177 (2004).
[135] A. Sternbeck and M. Muller-Preussker, Phys. Lett. B **726**, 396 (2013).
[136] G. Alexanian and V. Nair, Phys. Lett. B **352**, 435 (1995).
[137] R. D. Pisarski, Phys. Rev. D **74**, 121703 (2006).
[138] A. Dumitru, Y. Guo, Y. Hidaka, C. P. K. Altes, and R. D. Pisarski, Phys. Rev. D **83**, 034022 (2011).
[139] A. Dumitru, Y. Guo, Y. Hidaka, C. P. K. Altes, and R. D. Pisarski, Phys. Rev. D **86**, 105017 (2012).